19th Brazilian Congress of Thermal Sciences and Engineering
November 06th-10th, 2022, Bento Gonçalves - RS - Brazil

ENC-2022-0118
THERMODYNAMIC ANALYSIS OF AN ORGANIC RANKINE CYCLE INTEGRATED WITH LATENT HEAT STORAGE HARNESSING SOLAR THERMAL ENERGY FOR POWER GENERATION

Daniel Rubano Barretto Turci
Kleber Marques Lisboa
Universidade Federal Fluminense - Rua Passo da Pátria, 156 - Sala 206-D Bloco E Niterói, Rio de Janeiro, Brazil - Cep 24210-240.
daniel_turci@id.uff.br
kmlisboa@id.uff.br

Abstract
This paper aims to investigate the thermodynamic performance yielded by integrating solar collectors with a thermal energy storage system (TES) based on phase change material (PCM), and an organic Rankine cycle (ORC) for power generation. Theoretical calculations employing simplified lumped models for each component are carried out using the Wolfram Mathematica® platform. The so-called direct solar organic Rankine cycle system configuration (DSOS) is considered in this study, in which the ORC working fluid is vaporized directly in the solar collectors, for the associated reduction in the overall irreversibility of the integrated system as compared with the use of an intermediary fluid in the solar collector. R245fa is chosen as working fluid due to its favorable thermophysical properties and environmental-friendly characteristics. Evacuated flat plate collectors (EFPC) are chosen to harvest solar energy and their total area is fixed at 212.4 m². The models and methodologies are verified and validated with theoretical and experimental data, respectively, available in the literature for similar integrated systems. Averaged solar irradiation data taken from the Brazilian National Meteorology Institute (INMET) database for the city of Niterói, Rio de Janeiro, Brazil, is used as input. Performance metrics, such as net power generation, stored energy, and thermal efficiency are analyzed for typical summer and winter weeks of the year. The performance of the integrated system with and without the latent heat storage system are analyzed separately to probe the viability of its use and of the methodology proposed. This study intends to address a major limitation of solar systems, that is, the intermittency of its source, by proposing the use of thermal storage, thereby easing its adoption as a baseload energy source and the phase out of fossil fuels and other harmful alternatives.

Keywords: *Energy Efficiency, Solar Energy, Organic Rankine Cycle, Thermal Energy Storage System, Phase Change Materials.*

1. INTRODUCTION

According to the current World Energy Outlook report of the International Energy Agency (IEA, 2021), the most conservative projection estimates an increase of approximately 30% in electricity demand by 2030, and 80% by 2050, jumping from the current 23,300 TWh of electricity/year to approximately 42,000 TWh by 2050. In this context, the continuous growth in energy demand, associated with the possible scarcity of non-renewable energy resources and the strong environmental impact caused by them, represents one of the current most urgent global challenges (Rahbar et al., 2017). It becomes evident, therefore, the need for the development and improvement of technologies that use renewable and non-polluting resources, in order not only to meet the growing demand, but also to guarantee a clean and sustainable future for the next generations.

Among renewable and non-polluting sources, solar energy stands out as one of the most promising due to its abundance, inexhaustibility, and exploitability around the world (Rahbar et al., 2017). Furthermore, it is estimated that the sun constantly radiates about $4x10^{26}$ W of energy, $8x10^{16}$ W of which reach the surface of the earth (Rahbar et al., 2017), thus, in only one hour, the amount of energy input into the planet from the sun (80,000 TWh) is 3 times greater than the entire world demand for electricity registered in the year 2020 (23,300 TWh). However, the intermittence of the solar source remains the major constraint to its large-scale adoption (Nazir et al., 2019). Current commercial alternatives for electrochemical energy storage, such as batteries, are still costly, pose a relevant environmental risk, and are practically limited to large enterprises (Nazir et al., 2019).

In this context, thermal energy storage devices (TES) have been studied with special interest due to their potential and relatively low cost (Nazir et al., 2019). More specifically, the storage of heat through materials in phase change (phase change material or PCM) has been evaluated as one of the most promising for the effective use and integration with renewable resources (Alvi et al., 2020; Nazir et al., 2019). PCMs are particularly advantageous due to their high-energy density, and the capacity to release energy isothermally (Dutil et al., 2011). Moreover, recent studies pointed out that an exergetic efficiency of about 95% can be achieved with PCMs (Nazir et al., 2019).

To harness solar energy using a thermal storage system, a thermodynamic cycle may be employed to convert the energy harvested into electricity. Recent studies suggest the possibility of achieving stable and uninterrupted generation of electrical energy over long periods of time through the integration of thermal storage units to an organic Rankine cycle (ORC) powered by solar energy (Alvi et al., 2020). In fact, organic Rankine cycles have been the subject of numerous studies due to their potential use in distributed generation grids, and their adaptability to heat sources with low and medium temperatures (60–350 °C), being, for example, successfully employed in several geothermal plants (Rahbar et al., 2017; Delgado-Torres and García-Rodríguez, 2010). The possibility of changing the organic working fluid yields a flexibility not possible with conventional water steam cycles (Delgado-Torres and García-Rodríguez, 2010). In addition, ORC features conveniences such as simplicity, small size, low capital and maintenance cost, and high reliability compared to water steam plants (Rahbar et al., 2017).

Alvi et al. (2020) indicate that a temperature of approximately 100°C would be sufficient to operate an ORC integrated with solar collectors. Furthermore, their work concludes that the arrangement of a complete system, including PCM, in the configuration of direct steam generation (direct solar organic Rankine cycle system or DSOS), that is, utilizing the solar collectors as evaporators in the ORC, yields larger efficiencies and, consequently, greater net power generation, when compared to the conventional indirect generation configuration. One of the reasons is the large irreversibility associated with the interposition of a heat exchanger between the working fluids of the ORC and the solar collector (Alvi et al., 2020). Finally, Alvi et al. (2020) points out that despite the availability of works that study different configurations for solar ORC, few researchers have focused on the analysis of integration with thermal storage devices.

In short, motivated by the immense potential of the solar resource, and all the socio-environmental issues that encompass the current conjuncture of sustainability and clean energy, this paper presents a thermodynamic analysis of a solar organic Rankine cycle system integrated with a PCM for power generation. A lumped thermodynamic analysis of the solar-collector-PCM-ORC integrated system is carried out. The models and methods employed in each component are thoroughly verified and validated against theoretical and experimental data available in the literature. Time series for the power generated and thermal efficiency along typical summer and winter weeks for the city of Niterói, Rio de Janeiro, Brazil, are provided and critically analyzed to determine the viability of the proposed system and evaluate the performance advantages introduced by the latent thermal energy storage system.

2. MODEL AND METHODS

2.1 Solar organic rankine cycle

DSOSs systems with and without PCMs as thermal energy storage are considered. The schematic diagrams of the systems proposed are shown in Fig. 1. Both are composed of evacuated flat plate collectors (EFPCs), low pressure turbine, electric generator, condenser, and pump. The basic difference between them is the presence of a PCM tank and an open heater to mix the output fluid from the PCM with the condensed fluid coming from the pump. The working fluid is the refrigerant R245fa in both configurations.

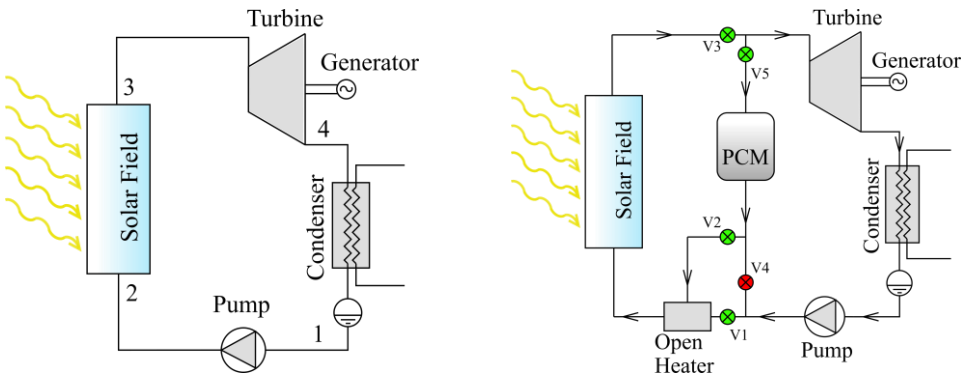

Figure 1. Direct solar organic Rankine cycle system (DSOS) configuration without energy storage system (left) and with energy storage system based on PCM during charging mode (right).

The DSOS configuration with PCM also presents a set of five valves, V1, V2, V3, V4, and V5 (Fig. 1), which are activated depending on the solar radiation and system circumstances. Thus, five operation modes, OM1, OM2, OM3, OM4 and OM5 are made possible: OM1 is the "system off" mode, where the solar energy absorbed by the collectors is zero or it is not enough to vaporize the working fluid and drive the turbine for power generation. Generally, OM1 is the condition for the night period (PCM discharged) and for irradiations below the operational minimum for vaporizing the working fluid of 100 W/m². OM2 is the "direct generation mode", which is activated when the irradiation is high enough to produce power (above 100 W/m²), but not high enough to charge the PCM. During the OM2 mode the pump constantly adjusts its mass flow rate, depending on the solar radiation, to keep the collector output temperature at 67°C. This mode is achieved by opening the valves V1 and V3 and closing the others. The OM3 or the "direct generation PCM charging" mode is activated following OM2, when the solar irradiation goes above 566 W/m², that is when the power produced by the OM2 mode reaches approximately 4 kW. Notably, the mass flow rate diverted to the PCM during OM3 (through the valve V5) depends on the solar radiation, that is, the higher the solar energy available, the higher the PCM mass flow rate diverted, and consequently, the higher the energy stored in the PCM. Also, during the OM3 mode the collectors output temperature is set to 100°C, so the pump also adjusts its flow to keep it constant. OM3 mode can be achieved by closing V4 and opening the others. The OM4 mode, or the "direct generation PCM support mode" is obtained by closing V2 and opening the others. In this circumstance, the mass flow rate within the PCM inverts its direction and the PCM begins to discharge, generating a maximum power of 4 kW together with the solar system. This operation mode is activated when the solar irradiation falls to a value between 100 W/m² and 566 W/m². For the OM4 mode, the collectors output temperature is set back to 67°C, which is the same as the melting temperature of the PCM. Finally, the OM5 mode, or the "PCM generation mode" is activated on zero or very low irradiations (below approximately 100 W/m²), so the collector field might not be able to vaporize the working fluid anymore, and the PCM feeds the turbine alone until its total discharge. This mode is obtained by closing V1, V2 and V3, and opening V4 and V5.

For the system solar irradiation input, the model proposed considers hourly and horizontal global radiation experimental data, which is converted to the inclined plane of the EFPC solar field. 90 EFPC collectors are considered for solar energy absorption, accounting for 212.4 m² of gross area.

The adopted control strategy of constantly adjusting the mass flow rate and monitoring the outlet temperature in the collectors has the objective of stabilizing the *per mass* power production by keeping a constant temperature at the inlet of the turbine, depending on the configuration and the operating mode. Moreover, for the configuration mode with PCM, a target of 4 kW of stable power generation is aimed for as long as possible. A numerical code on the Wolfram Mathematica® platform has been written to implement the solution methodology to be described.

2.2 Solar radiation

To estimate the total solar irradiation that reaches the collector's array (I_T), the HDKR model (Hay, Davies, Klucher, Reindl model) for inclined plane and anisotropic sky is used, according to the following (Duffe, 2020):

$$I_T = (I_b + I_d A_i) R_b + I_d (1 - A_i) \left(\frac{1 + \cos\beta}{2}\right) \left[1 + f \sin^3\left(\frac{\beta}{2}\right)\right] + I \rho_g \left(\frac{1 - \cos\beta}{2}\right) \quad (1)$$

where I is the hourly total solar irradiation on a horizontal surface (experimental measurement, in J/m²); I_b is the beam radiation component; I_d stands for the diffuse radiation; A_i is the anisotropy index; R_b is the ratio of beam radiation on a tilted plane to that on horizontal surface; ρ_g is the ground reflectance; f is a factor calculated as $\sqrt{I_b/I}$; and β is the slope angle of collector's array relative to the horizontal plane, considered as the same as latitude angle for maximum annual energy availability (Duffe, 2020).

Geographic, atmospheric, and local conditions data from open repositories are considered to carry out the analysis. The database used in this work is from the Brazilian National Meteorology Institute (INMET, 2022), for the city of Niterói, Rio de Janeiro. The coldest and hottest months of the year of 2020 (July and February, respectively) were evaluated as reference months for the study. Moreover, as the simulation considers a system positioned at the south hemisphere, the surface azimuth angle (γ) is set to 180°, that is, with the collectors pointing to the geographic north. Table 1 present the main fixed input parameters of this study.

Table 1. Input parameters used in the simulation procedure for irradiation on tilted plane.

Solar Constant (G_{sc})	**Latitude** (ϕ)	**Surface Slope** (β)	**Surface Azimuth Angle** (Υ)	**Ground Reflectance** (ρ_g)
1367 W/m²	-22.8°	22.8°	180°	0.5

2.3 Solar collectors

A set of fixed flat plate collectors of the vacuum tube type (EFPC) is chosen in this study. For calculation purposes, the technical data of the model VITOSOL-300 TM from Viessman manufacturer, with a gross area of 2.36 m², is used. The associated parameters are obtained from the datasheet provided by the manufacturer and certified test results (TUVRheinland, 2013). The fraction of irradiated energy transferred to the working fluid for a single collector is obtained as (Duffe, 2020):

$$Q_{cl} = \eta_{cl} I_T A_a \tag{2}$$

where A_a is the aperture area; and η_{cl} is the efficiency of the collector relative to A_a. I_T is the total solar irradiation that reaches the plane of the collector (J/m²) per hour. The parameter η_{cl} is calculated as the instantaneous efficiency according to the relationship (Duffe, 2020):

$$\eta_{cl} = a_0 - a_1 \frac{\Delta T_m}{G_T} - a_2 \frac{\Delta T_m^2}{G_T} \tag{3}$$

where a_0, a_1 and a_2 are the optical efficiency, linear heat loss coefficient and quadratic heat loss coefficient, respectively. G_T is the total solar irradiance on the collector plane (W/m²), calculated as the average value of $I_T/3600$. The parameter ΔT_m is the true mean fluid temperature difference, which can be approximated as (Duffe, 2020):

$$\Delta T_m = \frac{(T_i + T_o)}{2} - T_a = T_{avg} - T_a \tag{4}$$

where T_a is the ambient temperature, according to the database; T_i and T_0 are the inlet and outlet temperature of the working fluid in the collector; and T_{avg} is the average inlet-outlet temperature. Table 2 summarizes values for the parameters used in the simulation of the collector's field.

Table 2. Parameters for the simulation of the collector's array (TUVRheinland, 2013).

Simulation fixed parameters - Collectors	**Value**
Optical efficiency (a_0)	0.769
Linear heat loss efficiency (a_1)	1.256 W/(m² K)
Quadratic heat loss coefficient (a_2)	0.005 W/(m² K²)
Gross area of the collector (A_g)	2.36 m²
Aperture area of the collector (A_a)	1.6 m²
Maximum allowable pressure (P_{max})	600 kPa
Total number of collectors (n)	90
Number of collectors in series (n_{series})	30
Number of lines in parallel ($n_{parallel}$)	3

The collector model selected for the simulation allows for a maximum pressure of 600 kPa. This value was taken into account when selecting the working fluid (R245fa), which should meet the system requirements, such as the outlet temperature, within the allowable pressure. In addition, since there is a phase change process of the working fluid for the direct vapor generation, the efficiency of the collector must be evaluated at every stage (subcooled liquid preheating, evaporating, and vapor superheating) separately (Delgado-Torres and García-Rodríguez, 2010). Thus, the heat transfer rate from the collector to the working fluid can be calculated as (Delgado-Torres and García-Rodríguez, 2010):

$$\dot{Q}_{cl \to fluid} = \dot{Q}_{preheat} + \dot{Q}_{evap} + \dot{Q}_{superheat} \tag{5}$$

where $\dot{Q}_{preheat}$, $\dot{Q}_{evap}$ and $\dot{Q}_{superheat}$ are the heat transfer rates absorbed by the working fluid in the preheating, evaporation, and superheating process, respectively.

For the calculation of the collector efficiency during the evaporating process $\eta_{cl,evap}$, the value T_{avg} is taken as the evaporation temperature. The efficiencies of the collector at the preheating and the superheating stages, $\eta_{cl,preheat}$ and $\eta_{cl,superheat}$, are calculated with Eq. (3). Moreover, according to Delgado-Torres and García-Rodríguez (2010), every heating stage has an associated aperture area that can be calculated relative to the corresponding working fluid stage:

$$A_{a,preheat} = \frac{\dot{Q}_{preheat}}{G_T \eta_{cl,preheat}} = \frac{\dot{m} \Delta h_{2-2'}}{G_T \eta_{cl,preheat}} \tag{6}$$

$$A_{a,evap} = \frac{\dot{Q}_{evap}}{G_T \eta_{cl,evap}} = \frac{\dot{m} \Delta h_{2'-3'}}{G_T \eta_{cl,evap}} \tag{7}$$

$$A_{a,superheat} = \frac{\dot{Q}_{superheat}}{G_T \eta_{cl,superheat}} = \frac{\dot{m}\Delta h_{3\prime-3}}{G_T \eta_{cl,superheat}} \tag{8}$$

where $\dot{m}$ is the mass flow rate within the collector; $\Delta h_{2-2\prime}$ is the enthalpy difference between states 2 and 2'; $\Delta h_{2\prime-3\prime}$ is the enthalpy difference between states 2' and 3'; and $\Delta h_{3\prime-3}$ is the enthalpy difference between states 3' and 3, according to Fig. 3. Thus, the collector global efficiency is given by (Delgado-Torres and García-Rodríguez, 2010):

$$\eta_{cl,g} = \frac{\dot{Q}_{cl\rightarrow fluid}}{G_T A_a} = \Delta h_{2-3}\left(\frac{\Delta h_{2-2\prime}}{\eta_{cl,preheat}} + \frac{\Delta h_{2\prime-3\prime}}{\eta_{cl,evap}} + \frac{\Delta h_{3\prime-3}}{\eta_{cl,superheat}}\right)^{-1} \tag{9}$$

From a practical point of view, the thermal load of a system is generally supplied by setting several lines in parallel and some collectors in series on each line (Martínez-Rodríguez et al., 2019). In this study, 30 collectors in series (n_{series}) and 3 lines in parallel ($n_{parallel}$) are analyzed. Thus, the Eq. (2) can be rewritten as follows

$$\dot{Q}_{cl,series} = \eta_{cl,g} G_T (n_{series} A_a) \tag{10}$$

where $\dot{Q}_{cl,series}$ is the heat transfer rate absorbed by the working fluid in each line of collectors in series.

Finally, for the adjustable mass flow rate to maintain a fixed output (Martínez-Rodríguez et al., 2019) according to the irradiation and ambient conditions, the following equation is considered:

$$\dot{m}_{sys} = n_{parallel}\left(\frac{\dot{Q}_{cl,series}}{h_3 - h_2}\right) \tag{11}$$

where $\dot{m}_{sys}$ is the total mass flow rate of the system.

2.4 Latent Heat Storage

A simplified model of the thermal energy storage system (TES) is adopted to analyze the complete system integration and the impact on the energy production. In this way, hypotheses such as instantaneous local equilibrium, uniform heat transfer along the contact surface, adiabatic boundary, and constant thermophysical properties are adopted. Furthermore, natural convection effects that may occur due to the temperature difference inside the PCM (Alvi et al., 2020) are neglected. Figure 2 illustrates a schematic of the PCM model.

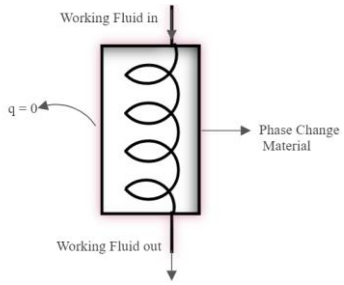

Figure 2. Diagram of the latent heat storage system

The heat transfer between the PCM and the working fluid during the steady process can be expressed as follows (Lim et al.,1992):

$$\dot{Q}_{PCM} = \dot{m}_{pcm} c_p \left(T_{i,pcm} - T_m\right)\left(1 - e^{-(UA_c)/(\dot{m}_{pcm} c_p)}\right) \tag{12}$$

$$\dot{Q}_{PCM} = \dot{m}_{pcm}\left(h_{i,pcm} - h_{o,pcm}\right) \tag{13}$$

where $T_{i,pcm}$ is the working fluid inlet temperature of the PCM; the melting temperature depends on the material chosen and is given by T_m; $\dot{m}_{pcm}$ is the mass flow rate of the working fluid through the PCM; $h_{i,pcm}$ and $h_{o,pcm}$ are the enthalpies of the working fluid at the PCM inlet and outlet, respectively; the thermal conductance UA_c is assumed to be constant and estimated as 1500 W/K (Alvi et al., 2020; Incropera and de Witt, 2007), where A_c is the contact area between the working fluid and the PCM, and U is the overall heat transfer coefficient; c_p is the working fluid specific heat at constant pressure.

The PCM material is primarily chosen based on its melting temperature (T_m) (Prashant Verma and Singal, 2008). Table 3 specifies the PCM selected in this study.

Table 3. Thermophysical properties of the PCM used for the current study (Prashant Verma and Singal, 2008).

PCM Thermo-Physical properties	
Compound	67.1% Napthalene + 32.9% benzoic acid
Melting Temperature (T_m)	67 °C

2.5 The organic Rankine cycle

In general, the Rankine cycle is widely used in power generation systems (Rahbar et al., 2017). Figure 3 represent the T-S diagram for a simple organic Rankine cycle system.

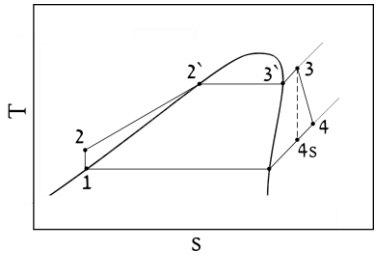

Figure 3. T-S diagram of the DSOS configuration without thermal energy storage.

The process in the evaporator, from state 2 to state 3, is divided into three parts: firstly, the subcooled liquid (state 2) is heated to saturated liquid (state 2'); then the latent heat transfer occurs, producing saturated steam (state 3'); finally, the steam is superheated (state 3), which is to be expanded in the turbine to produce power. The condenser is responsible for taking the turbine outlet superheated fluid (state 4) and condensing it back to state 1, where the pump adds pressure to the fluid for a new cycle.

The model adopted for the ORC in this study assumes quasi-steady one-dimensional flow and negligible pressure drop. Moreover, irreversibilities in the turbine and pump are taken into account. The efficiency of the electric generator is assumed to be 85%. The parameters used in the simulation are based on a similar study for solar application (Alvi et al., 2020), and are presented in Tab. 4. The ORC working fluid adopted is the refrigerant R245fa, due to its favorable thermophysical properties and environmental-friendly characteristics (Wang et al., 2010).

Table 4. Entry data for the analysis of the ORC system.

Configuration	**Collectors array outlet temperature** ($T_{cl,o}$)	**Degree of superheating at turbine inlet** (ΔT_{sup})	**Condensation temperature** ($T_{condens}$)	**Turbine isentropic efficiency** (η_t)	**Pump isentropic efficiency** (η_b)
Without PCM	72 °C	3 ºC	25 ºC	0.8	0.6
With PCM – OM2, OM4 and OM5	67°C	3 ºC	25 ºC	0.8	0.6
With PCM – OM3	100°C	36 ºC	25 ºC	0.8	0.6

The power generated by the turbine and consumed by the pump is given by:

$$\dot{W}_t = \dot{m}_{ORC}\left(h_{t,i} - h_{t,o}\right) \tag{14}$$

$$\dot{W}_b = \dot{m}_{ORC}\left(h_{b,o} - h_{b,i}\right) \tag{15}$$

where $\dot{m}_{ORC}$ represents the mass flow rate of the working fluid during power generation; $h_{t,i}$ and $h_{t,o}$ the turbine inlet and outlet enthalpies; and $h_{b,i}$ and $h_{b,o}$ the pump inlet and outlet enthalpies, respectively.

The isentropic efficiencies of the turbine and pump are defined as:

$$\eta_t = \frac{h_{t,i} - h_{t,o}}{h_{t,i} - h_{t,os}} \tag{16}$$

$$\eta_b = \frac{h_{b,os} - h_{b,i}}{h_{b,o} - h_{b,i}} \tag{17}$$

where $h_{t,os}$ and $h_{b,os}$ are the turbine and pump output enthalpies considering an isentropic process.

The heat transfer rate required by the ORC in the heating process can be determined as:

$$\dot{Q}_{ORC} = \dot{m}_{ORC}(h_{t,i} - h_{b,o}) \tag{18}$$

In this way, the net power delivered is calculated considering the efficiency of the electric generator and deducting the pumping power, as follows:

$$\dot{W}_{net} = \dot{W}_t \eta_g - \dot{W}_b \tag{19}$$

where η_g corresponds to the generator efficiency.

The cycle efficiency is computed as:

$$\eta_{ORC} = \frac{\dot{W}_{net}}{\dot{Q}_{ORC}} \tag{20}$$

Finally, the system efficiency is obtained multiplying η_{ORC} by the efficiency of the collector (Alvi et al.,2020):

$$\eta_{sys} = \eta_{ORC}\eta_{cl,g} \tag{21}$$

3. RESULTS AND DISCUSSION

Results obtained with the Wolfram Mathematica® simulation code for the ORC-solar system are presented, analyzed and discussed in this section. Since it uses hourly based experimental data from Brazilian National Meteorology Institute (INMET) for solar radiation, a time step of 1h is used for the whole simulation process. Moreover, the study considers two different scenarios: the behaviors of the system for a representative week in summer, and for a representative week in winter. For the summer, the data employed is for the week between 15th and 21rst of February, and, for the winter, for the week between 15th to 21rst of July, both from the year 2020.

3.1 Validation of numerical model

The ORC model has been verified and validated with theoretical and experimental data available in the literature for similar systems. Table 5 and Table 6 show the results from the literature and the comparison with the values obtained through the methodology and computational code developed in this work. Compared with the numerical results from Alvi et al. (2020), that evaluates an ORC-solar integrated system using R245fa as working fluid and a PCM for thermal storage, the deviation was limited to 6% as evident from Tab. 5. In comparison with the experimental results from Catapano et al. (2022), that uses R134a as the working fluid to study the performance of an integrated ORC prototype and a latent thermal energy storage system for waste heat recovery, a relative difference of up to 10% is found from the results of the proposed methodology. The favorable comparisons with two independent results enhances the confidence on the reliability and accuracy of the model and methodology for the analysis of organic Rankine cycles integrated with solar collectors and latent heat storage.

Table 5. Verification with theoretical data from a numerical work on ORCs (Alvi et al.,2020).

Working fluid: **R245fa**	Total power	Pump consumption	Net power	Efficiency
(Alvi et al., 2020)	-	-	14288 W	11.6%
ORC Simulation	14401 W	921 W	13480 W	11.0%
Relative difference	-	-	6%	5%

Table 6. Validation with experimental data for ORCs (Catapano et al., 2022).

Working fluid: **R134a**	Total power	Pump consumption	Net power	Efficiency
(Catapano et al., 2022)	1352 W	164 W	1187 W	3.9%
ORC Simulation	1380 W	178 W	1202 W	3.5%
Relative difference	2%	9%	1%	10%

3.2 Solar radiation during typical summer and winter weeks on the collectors

The variation in total solar irradiation on the plane of the collector for the representative week of winter and summer are shown in Fig. 4. Remarkable differences can be noted from the analysis: the summer week shows an

average of 12 hour of solar radiation per day, while the winter week has 2 hours less per day on average. A typical summer day starts with significant radiation at 7 a.m. and sustains it until 6 p.m., while relevant solar incidence in a typical winter day goes at most from 8 a.m. to 5 p.m.. In addition, during a clear sky summer day (day 4, 5 and 6 of Fig. 5), the solar irradiance might go above 1000 W/m² at around 1 p.m., while, on a winter day, the maximum solar irradiance never exceeds the 957 W/m² verified at day 4.

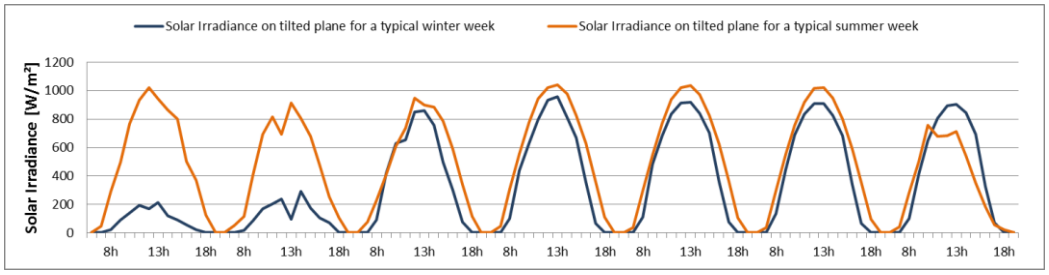

Figure 4. Solar radiation for a typical week of winter and summer comparison.

3.3 Analysis of the integrated system of solar collectors and organic Rankine cycle without PCM

The net power outputs and system efficiencies for the DSOS configuration without PCM are shown in Fig. 5 and Fig. 6 for both the summer and winter week periods adopted for this study. As it was expected, the maximum power output is achieved on a summer day, totaling 8.3 kW during the radiation peak hour at day 4. The corresponding mass flow rate is 0.49 kg/s, and a system efficiency of 5.6% was attained.

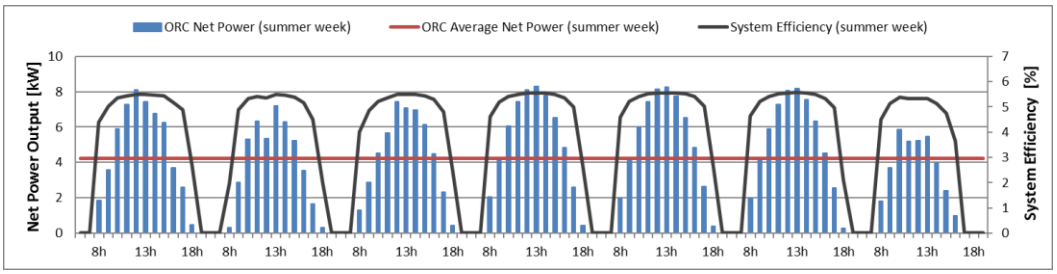

Figure 5. Variation in net power output and system efficiency without PCM during a typical summer week.

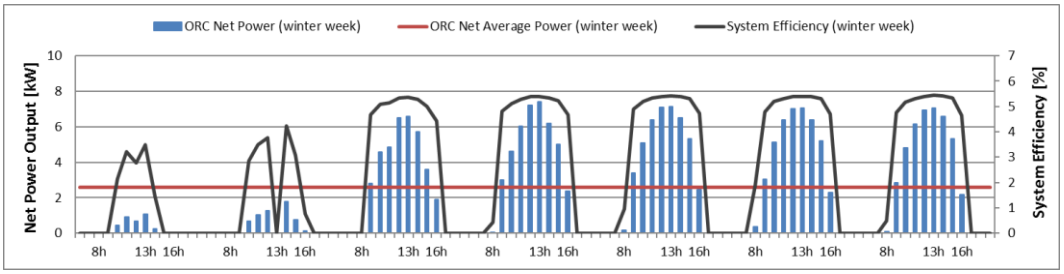

Figure 6. Variation in net power output and system efficiency without PCM during a typical winter week.

The winter week also presents its maximum parameters at day 4, producing a total of 7.4 kW of power output during the radiation peak hour, 0.44 kg/s of mass flow rate, and a system efficiency of 5.4%. Notably, the difference on the maximum values between the summer and winter weeks are not too significant; for the power output and system efficiency, the summer maximum is approximately 12.2% and 3.7% larger than the winter maximum, respectively. However, a larger difference can be verified when analyzing the average net power output of the system between the hours of 7 a.m. to 6 p.m. For the summer, an average of 4.2 kW of power output is obtained, while, in the winter, this value falls to 2.6 kW, accounting for 62% of difference. This greater difference can be explained by Fig. 4, which shows that a typical summer day has an average of 2 hours of significant radiation more than the typical winter day. Due to this fact, the total energy production difference between the summer and the winter week is also pronounced, with the summer week summing up to 355 kWh of energy produced, while, in the winter week, this value drops to 216 kWh of energy, thereby, approximately 64% more energy is produced during the summer week than in the winter week.

3.4 Analysis of the integrated system of solar collectors and organic Rankine cycle with PCM

The net power output and the system stored energy for the DSOS configuration with PCM are shown in Fig. 7 and Fig. 8 for both the summer and winter week periods. For this configuration, the system is designed to maintain a target of 4 kW of stable power generation for as long as possible. As expected, the summer week showed better results when compared to the winter week in this context. For the summer, the PCM charging mode starts at around 10 a.m., and keeps charging until 4 p.m. on a clear day (days 4, 5 and 6), while for the winter week, on its three best days (day 4, 5 and 6) it starts at 10 a.m. and goes at most up to 3 p.m. Also, due to the higher solar irradiation and longer days, the summer week showed a considerably higher capacity of storing energy, reaching a maximum of 603 MJ at day 4, against a maximum of 415 MJ of stored energy for the winter week at day 5. The difference of the energy storage capacity between summer and winter is also reflected on longer generation periods for the summer. Figure 7 shows that during the summer week in 4 out of 7 days the system keeps generating power up to 8 p.m., while during the winter week it is restricted to a maximum of 6 p.m.

During the high irradiation hours (around 11 a.m. to 2 p.m.) the power output might go slightly above 4 kW (Fig. 8 and 9) due to the limitation of the pump, which is adjusting its flow rate to keep a constant temperature at the collector's outlet. For the summer, a maximum power output of 4.96 kW is verified at day 4, while for the winter period the higher value is 4.47 kW at day 4. In addition, the mass flow rate passing through the PCM is higher during the summer week than during the winter week, which confirms the trend of storing more energy during the summer periods. Regarding the total amount of energy produced along the weeks, the simulation yielded 316 kWh and 193 kWh produced for the summer and winter periods, respectively.

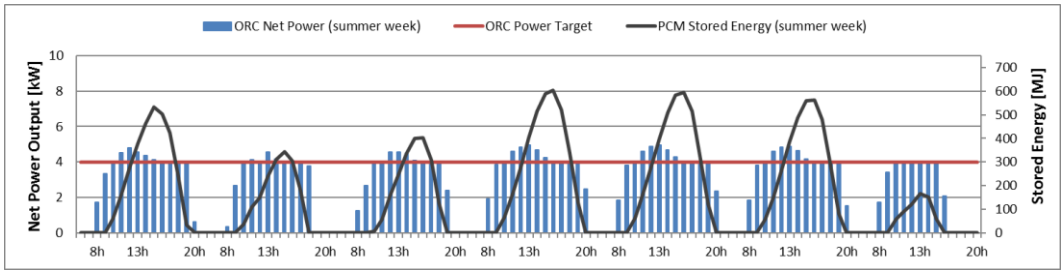

Figure 7. Variation in net power output and PCM load during a typical summer week.

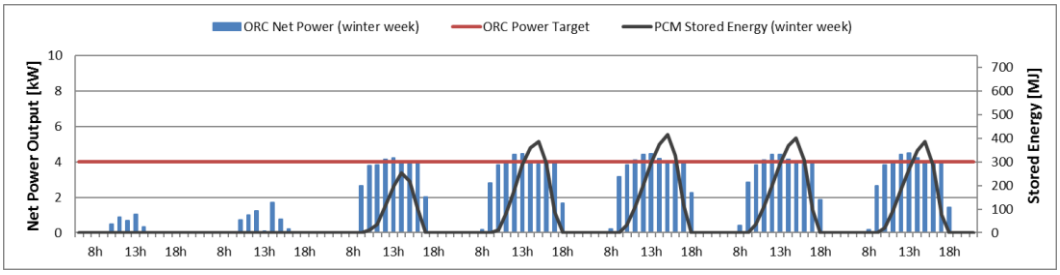

Figure 8. Variation in net power output and PCM load during a typical winter week.

4. CONCLUSIONS

The thermodynamic performance of the DSOS with and without PCM for typical summer and winter weeks is analyzed in this study. A mathematical model is developed for the integration of the EFPC collector field, ORC, and PCM. The mass flow rate of the system together with the outlet temperature of the collectors are used as control parameters to keep the turbine inlet temperature constant, thus allowing the prediction of the system efficiency and energy production. First, the performance analysis of the system without PCM is carried out to determine the potential for power generation and the efficiency of the integrated system for summer and winter conditions. It is concluded from the results that the system without PCM reaches a maximum efficiency of 5.6% during the summer week, not markedly decaying the other days. Furthermore, despite the mild difference between the maximum solar irradiance observed in the summer and winter weeks, approximately 64% more energy would be produced in the summer week due to its longer days and greater average power outputs.

The performance of the ORC system integrated with a PCM for thermal energy storage is carried out in order to evaluate its potential employment as a baseload energy source. A target of 4 kW of power generation is set, and the control parameters are adjusted with time, aiming at maintaining a constant and stable generation for as long as possible. It is concluded from de results that the use of PCM could extend the operation time at a high-power production

to up to 8 p.m. during summer, and up to 6 p.m. during winter. Thus, the use of PCM on the methodology proposed showed good capacity of reducing the power generation peaks at higher irradiation, yet low demand, hours, and increasing the power generation to a desirable level at low or zero irradiation hours during demand peaks typically ocurring between 6 p.m. to 9 p.m. This characteristic makes the use a PCM integrated with a solar system and an ORC a potentially interesting alternative to mitigate the intermittency issue of renewable energy sources.

5. ACKNOWLEDGEMENTS

The authors wish to thank the National Oil Agency Human Resources Program (ANP-PRH, contract nº51 process: 046119), the Higher Education Personnel Improvement Coordination (CAPES), and Fundação Carlos Chagas Filho de Amparo à Pesquisa do Estado do Rio de Janeiro (FAPERJ) for supporting this research work.

6. REFERENCES

Alvi, J.Z., Feng, Y., Wang, Q., Imran, M. and Junaid Alvi, 2020. "Modelling, simulation and comparison of phase change material storage based direct and indirect solar organic Rankine cycle systems". *Applied Thermal Engineering, 170*.

Bejan, A., 1996. *Entropy Generation Minimization - The Method of Thermodynamic Optimization of Finite-Size Systems and Finite-Time Processes.* Boca Raton, New York: CRC Press.

Catapano, F., Frazzica, A., Freni, A., Manzan, M., Micheli, D., Palomba, V., Sementa, P. and Vaglieco, B.M., 2022. "Development and experimental testing of an integrated prototype based on Stirling, ORC and a latent thermal energy storage system for waste heat recovery in naval application". (Elsevier, Ed.) *Applied Energy, 311*.

Delgado-Torres, A.M. and García-Rodríguez, L., 2010. "Analysis and optimization of the low-temperature solar organic Rankine cycle (ORC)". *Energy Conversion and Management, 51, Issue 12*, pp. 2846-2856.

Duffe, J.A., Beckman, W.A. and Blair, N., 2020. *Solar Engineering of Thermal Processes, Photovoltaics and Wind* (5ª ed.). Hoboken, New Jersey, Estados Unidos da América: John Wiley & Sons, Inc.

Dutil, Y., Rousse, D.R., Salah, N.B., Lassue, S. and Zalewski, L., 2011. "A review on phase-change materials: Mathematical modeling and simulations". *Renewable and Sustainable Energy Reviews, 15, Issue 1*, pp. 112-130.

Incropera, F. P. and de Witt, D. P., 2007. "*Fundamentos de Transferência de Calor e de Massa*" (6ª ed.). John Wiley & Sons.

Instituto Nacional de Meteorologia (INMET). (s.d.). *Banco de Dados Meteorológicos do INMET*. Acessed January 10, 2022, available at Instituto Nacional de Meteorologia (INMET): https://bdmep.inmet.gov.br/

International Energy Agency (IEA)., 2021. *World Energy Outlook 2021*. IEA.

Lim, J. S., Bejan, A., and Kim, J. H., 1992. "Thermodynamic Optimization of Phase-Change Energy Storage Using Two or More Materials". *ASME Digital Collection, 114*.

Martínez-Rodríguez, G., Fuentes-Silva, A.L., Lizárraga-Morazán, J.R. and Picón-Núñez, M., 2019. "Incorporating the Concept of Flexible Operation in the Design of Solar Collector Fields for Industrial Applications". *Energies, 12, Issue 3*, 570.

Nazir, H., Batool, M., Osorio, F.J.B., Isaza-Ruiz, M., Xu, X., Vignarooban, K., Phelan, P., Inamuddin and Kannan, A.M. 2019. "Recent developments in phase change materials for energy storage applications: A review". *International Journal of Heat and Mass Transfer, 129*, pp. 491-523.

Prashant Verma, V., Singal, S.K., 2008. "Review of mathematical modeling on latent heat thermal energy storage systems using phase-change material". *Renewable and Sustainable Energy Reviews, 12, Issue 4*, 999-1031.

Rahbar, K., Mahmoud, S., Al-Dadah, R.K., Moazami, N. and Mirhadizadeh, S.A., 2017. "Review of organic Rankine cycle for small-scale applications". *Energy Conversion and Management, Volume 134*, pp. 135-155.

TUVRheinland., 2013. Licence Number 011-7S2192 R. *Summary of EN 12975 Test Result, annex to Solar Keymark Certificate*. Allendorf, Germany.

Wang, X.D., Zhao, L., Wang, J.L., Zhang, W.Z., Zhao, X.Z., and Wu, W., 2010. "Performance evaluation of a low-temperature solar Rankine cycle system utilizing R245fa". *Solar Energy, 84, Issue 3*, 353-364.

7. RESPONSIBILITY NOTICE

The authors are the only responsible for the printed material included in this paper.